APL Photonics

Ultra-sensitive refractive index gas sensor with functionalized silicon nitride photonic circuits

Cite as: APL Photonics **5**, 081301 (2020); https://doi.org/10.1063/5.0013577
Submitted: 13 May 2020 . Accepted: 12 July 2020 . Published Online: 12 August 2020

Giuseppe Antonacci, Jeroen Goyvaerts, Haolan Zhao, Bettina Baumgartner, Bernhard Lendl, and Roel Baets

COLLECTIONS

F This paper was selected as Featured

View Online Export Citation CrossMark

AMERICAN ELEMENTS
THE ADVANCED MATERIALS MANUFACTURER®
American Elements opens up a world of possibilities so you can **Now Invent!**
Over 15,000 certified high purity laboratory chemicals, metals, & advanced materials and a state-of-the-art Research Center. Printable GHS-compliant Safety Data Sheets. Thousands of new products. And much more. All on a secure multi-language "Mobile Responsive" platform.
Now Invent.™
The Next Generation of Material Science Catalogs
www.americanelements.com

© 2020 Author(s).

Ultra-sensitive refractive index gas sensor with functionalized silicon nitride photonic circuits

Cite as: APL Photon. 5, 081301 (2020); doi: 10.1063/5.0013577
Submitted: 13 May 2020 • Accepted: 12 July 2020 •
Published Online: 12 August 2020

View Online Export Citation CrossMark

Giuseppe Antonacci,[1,2,a)] Jeroen Goyvaerts,[1,2] Haolan Zhao,[1,2] Bettina Baumgartner,[3] Bernhard Lendl,[3] and Roel Baets[1,2]

AFFILIATIONS

[1] Photonics Research Group, INTEC, Ghent University-IMEC, Ghent 9052, Belgium
[2] Center for Nano- and Biophotonics (NB-Photonics), Ghent University, 9052 Ghent, Belgium
[3] Institute of Chemical Technologies and Analytics, TU Wien, A-1060 Vienna, Austria

[a)] **Author to whom correspondence should be addressed:** giuse.antonacci@gmail.com

ABSTRACT

Portable and cost-effective gas sensors are gaining demand for a number of environmental, biomedical, and industrial applications, yet current devices are confined into specialized labs and cannot be extended to general use. Here, we demonstrate a part-per-billion-sensitive refractive index gas sensor on a photonic chip based on silicon nitride waveguides functionalized with a mesoporous silica top-cladding layer. Low-concentration chemical vapors are detected by monitoring the output spectral pattern of an integrated unbalanced Mach-Zehnder interferometer having one coated arm exposed to the gas vapors. We retrieved a limit of detection of 65 ppb, 247 ppb, and 1.6 ppb for acetone, isopropyl alcohol, and ethanol, respectively. Our on-chip refractive index sensor provides, to the best of our knowledge, an unprecedented limit of detection for low gas concentrations based on photonic integrated circuits. As such, our results herald the implementation of compact, portable, and inexpensive devices for on-site and real-time environmental monitoring and medical diagnostics.

© 2020 Author(s). All article content, except where otherwise noted, is licensed under a Creative Commons Attribution (CC BY) license (http://creativecommons.org/licenses/by/4.0/). https://doi.org/10.1063/5.0013577

Gas sensing is a central task for a plethora of applications including medical diagnostics, pollution monitoring, and industrial quality process control. In medical diagnostics, for example, recent studies have suggested the use of gas sensors in breath analysis to detect diseases such as lung cancer[1] and diabetes.[2] Environmental safety monitoring has also been a topic of recent interest in the microelectronics sensing industry with regards to the miniaturization and cost benefits that go along with replacing the current technologies. Despite the presence of broad technological solutions for gas detection,[3–5] these typically rely on bulk devices that lack the affordability, robustness, and selectivity requirements for ensuring a global implementation outside specialized labs.

Demand for compact, cost-effective, and portable gas sensors has instigated new research on chip-scale silicon photonic devices. These promise benefits in terms of cost, size, and energy efficiency over traditional technologies that would potentially enable a wide spread and on-site adoption. In this regard, the novel silicon nitride (SiN) platform offers an excellent solution for sensing as a consequence of its broadband transparency window into the visible domain and the generally lower propagation losses compared to the SOI platform.[6] Given its versatility and the possibility to integrate multiple optical functionalities, the SiN platform has already enabled the implementation of several sensing devices for a variety of applications including biosensing,[7–9] Raman spectroscopy,[10–12] and absorption spectroscopy.[13] More recently, the SiN platform has further seen adoption for gas sensing. Celo *et al.*[14] first demonstrated the use of an integrated Mach-Zehnder interferometer (MZI) with SiN rib-waveguide structures coated with ~1 μm ZnO and TiO2 films to probe N_2 and CO_2. Similar approaches based on integrated MZIs realized with SOI and SiN platforms have been demonstrated with different types of coatings and waveguide structures to detect organic solvents,[15] ethanol vapors,[16] and methane,[17] reporting a limit of detection (LOD) in the order of tens of ppm. On-chip refractive index gas sensing has been further demonstrated

© Author(s) 2020

through microring resonators,[18–21] where a LOD down to 5 ppm has been recently achieved with acidic nano-porous aluminosilicate films for ammonia sensing.[22] Other emerging integrated approaches include absorption spectroscopy[23,24] and Raman spectroscopy.[25,26] These methods promise high selectivity, yet the requirement of signal-enhancement polymer coatings still limits their detection to specific binding analytes and to long enrichment times due to bulk diffusion.

In this Letter, we demonstrate a part-per-billion-sensitive on-chip gas sensor on a low-loss silicon nitride platform. Our sensing mechanism hinges on the refractive index change of the SiN waveguides evanescently exposed to the gas analytes across the openclad arm of an integrated unbalanced MZI. To enhance the instrumental sensitivity, the sensing arm of the MZI was coated with a functionalized mesoporous silica layer that preferentially adsorbs organic solvents. The light traveling along the exposed waveguides experiences a different refractive index when a gas vapor is adsorbed by the top-cladding mesoporous layer, resulting in a wavelength shift of the interference fringes generated by the MZI. We demonstrate this concept for a number of gas vapors including acetone, isopropyl alcohol (IPA), and ethanol.

Figure 1(a) illustrates the experimental setup. A supercontinuum (SC) laser source (NKT-EXR-4) was used in all experiments. The laser beam was directly coupled by means of a single mode fiber into the SiN waveguides of our photonic integrated circuit (PIC) through a grating coupler, which was designed for a 850 nm central wavelength to further enable the integration of high power VCSELs. The PIC was fabricated on IMEC's BioPIX platform [Fig. 1(b)], which provides a waveguide core thickness of 300 nm and is suited for applications targeting the near-infrared (700 nm–900 nm) range. The SiN used here is a PECVD nitride core of 1.89 refractive index, providing a relatively low material contrast with the 1.46 index of the SiO_2 cladding. This low material index contrast is particularly suited for sensing as the mode results to be less confined across the waveguide core, resulting in an extended evanescent tail, and therefore in a longer interaction length with the adsorbed gas analytes. As further demonstrated through the EU PIX4life pilot line,[27] the BioPIX SiN platform is also well-suited to design complex photonic components, including dual-etch staircase grating couplers, splitter modules, and low-loss on-chip spectrometers.

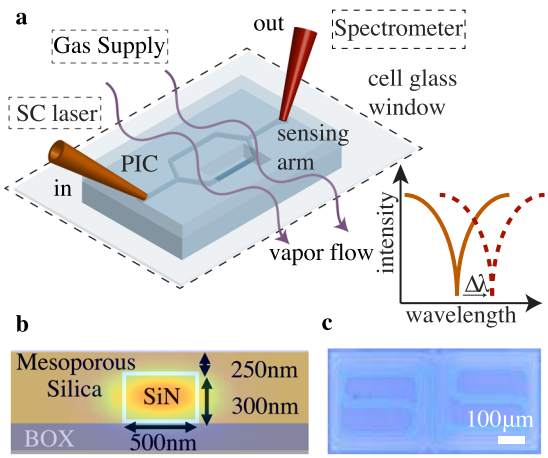

FIG. 1. Experimental setup (a). A supercontinuum (SC) laser beam was coupled into the SiN waveguides to probe the injected gas vapors. A polarization controller was used to ensure a TE mode propagating along the waveguides. The spectral readout was performed in real-time using a spectrometer. Cross section of our 300 nm SiN waveguides with functionalized mesoporous coating (b) and image of the integrated MZI (c).

The main building-block of the sensor is the integrated MZI [Fig. 1(c)]. The sensitivity of any generic unbalanced MZI is well-known to be described by[28,29]

$$\frac{d\lambda}{\lambda} = \frac{dn_{eff} L_{sens}}{|n_{g,sens} L_{sens} - n_{g,ref} L_{ref}|}, \tag{1}$$

where n_{eff} is the effective refractive index, n_g is the group index, and L_{sens} and L_{ref} are the MZI sensing and reference arm lengths, respectively. It is worth noting that Eq. (1) exhibits a strong dependence of the sensitivity on the arm lengths, which gives the opportunity to increase the sensitivity without dealing with the unpractically short Free Spectral Range (FSR), as in the case of balanced MZIs. On the other hand, for the strongly unbalanced MZI ($L_{ref} \ll L_{sens}$), Eq. (1) resumes the one describing the sensitivity of a ring resonator, as expected. We exploited this principle as well as the low-loss (typically ~ 0.5 dB/cm) of our SiN waveguides to design an unbalanced MZI with long interference arms (L_{ref} = 5.208 mm and L_{sens} = 5.416 mm). In turn, this results in an enhanced device sensitivity without detrimental influence neither on the signal contrast nor on the FSR, which was set to be ~1 nm for low-index coatings. The narrow FSR further provides the opportunity for further electro-optic integration of narrowband tunable lasers. Moreover, the strip waveguides of the sensing arm of the MZI were functionalized with an ordered mesoporous silica coating layer of ~500 nm thickness and with a 3D hexagonal structure.[30,31] Assuming a porosity of ~50% and using the Bruggeman effective medium approximation,[32] we estimated an effective medium refractive index of 1.21 in air. Moreover, the film was functionalized with hexamethyldisilazane to increase the hydrophobicity of the film.[33] This allowed for excluding the strong absorber water, while enhancing sensitivity toward organic molecules.

The use of a SC laser source enabled the employment of a broadband spectral analyzer (Agilent OSA 86140B) for direct and real-time readout of the output spectral interference pattern with a typical exposure time of 500 ms. The polarization of the SC source was controlled using a linear polarizer and a polarization controller acting as a half-wave plate to ensure coupling of the TE mode into the waveguides and to maximize the optical signal strength. Moreover, the PIC was kept enclosed inside a custom gas cell having an input and an output port for gas vapor flowing, and a transparent window to enable the optical incoupling and outcoupling. A gas generator (VICIMetronics Model 505) was employed to inject low (0.1 ppb-100 ppm) gas concentrations into the gas cell through a controlled permeation mechanism (supplementary material, Fig. 1a).

The sensor was first optically characterized to measure the device sensitivity and the optical stability in controlled environmental conditions. In more detail, the output spectral interference patterns of the MZI were acquired over time by the spectrometer, while the photonic chip was kept inside the gas cell at room temperature

© Author(s) 2020

(22 °C) with no gas vapor flowing. The output intensity profiles were first normalized from a typical baseline of ~−60 dBm and then fitted using a suitable sinusoidal function to track the location of the interference fringes of the MZI, as illustrated in Fig. 2(a). Figures 2(b) and 2(c) show a plot of the location in the spectral domain of an arbitrary interference fringe as a function of time and a histogram of the same dataset for a total of $N \sim 100$ independent repetitions, respectively. The results show good stability of the sensor over a time period of ~15 min, which was comparable to the data acquisition time period in our sensing experiments. From these measurements, we estimated a sigma of $\sigma = 0.0146$ nm, which sets the baseline noise level of our gas sensor.

Figure 3 shows the sensor response in terms of the relative wavelength shift over time after the exposure to acetone at different concentrations. To supply a broad range of concentrations to the gas cell, the gas generator was tuned either in temperature (setting the amount of gas permeation inside the supplier chamber) or in the diluent flow. For each measurement, the gas sensor was first exposed to the low gas concentration flow for 15 min to ensure a full adsorption cycle and thus a stabilization of the output spectral interference pattern. This process was then followed by an air diluent reflow for an equal amount of time to successfully return the optical signal to its original baseline, which was indicative of an effective resilience of the mesoporous silica coating that successfully resumed its original state upon desorption. The spectral interference patterns at the output of the MZI were recorded continuously by using the spectrometer with time steps of 1 s and fitted to finely track the wavelength shift of an arbitrary reference fringe. The results show clear visible signal responses of our gas sensor even at low (<1 ppm) gas concentrations, with spectral shifts that were well above the baseline noise level of the device.

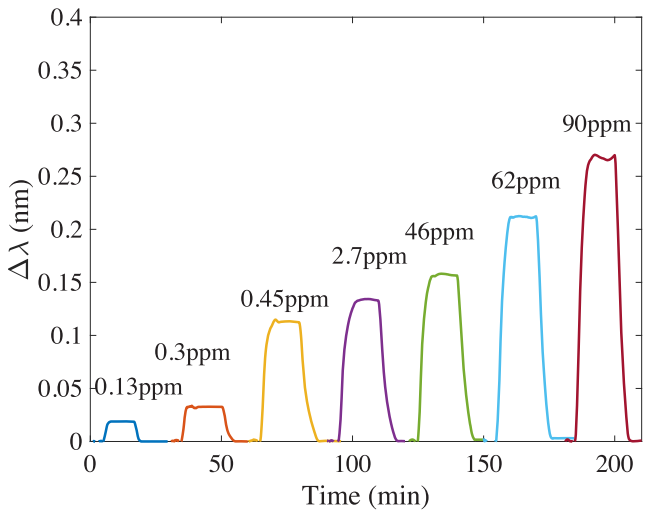

FIG. 3. Representative response curves of our gas sensor to the exposure to acetone vapors at different concentrations. Gas detection was accomplished by tracking the wavelength variation associated with a reference MZI fringe over time. The results show a clear response even at concentrations below a part-per-million scale.

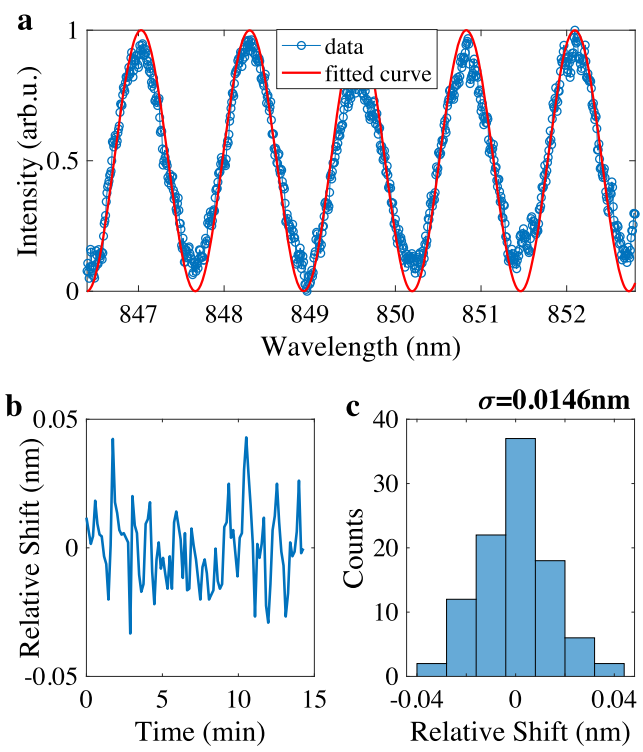

FIG. 2. (a) Normalized spectral interference pattern of the integrated MZI fitted with a sinusoidal function. (b) The wavelength variation of a fringe was monitored over a time period of 15 min to assess the sensor stability. (c) Histogram of the dataset, which gives a sigma of $\sigma = 0.0146$ nm as a baseline noise level on the extracted wavelength.

Generally speaking, MZIs are extremely sensitive devices to thermodynamic and environmental changes, including variations in temperature, pressure, and humidity. To ensure that the observed spectral shifts were given by the adsorption of the gas analytes rather than by a change in temperature caused by the permeation mechanism of the gas generator, we measured the sensor response at a fixed chamber temperature to the exposure of both normal air flow and acetone. The results illustrated in Fig. 1(b) of the supplementary material give convincing evidence of the negligible influence of the gas sensor on the heating mechanism occurring inside the permeation chamber of the gas generator. A similar test was performed to investigate the effect of humidity on the gas sensor (supplementary material, Fig. 2). As we expected, a change in the environmental humidity was reflected in a small step variation of the MZI fringes. However, exposure of gas vapors in altered humidity levels had no significant change in the relative spectral shift as compared to that given with the original humidity level.

To investigate the LOD and the sensitivity of our gas sensor, we swept the concentration of a number of gas vapors, namely, acetone, IPA, and ethanol, and record the wavelength shift of the MZI fringes. Figure 4 resumes the response curves of the gas sensor for the tested gas vapors. Wavelength shift values were obtained by averaging the spectral shifts given upon completion of the adsorption process. As shown, the sensor had a non-linear response to the exposure

© Author(s) 2020

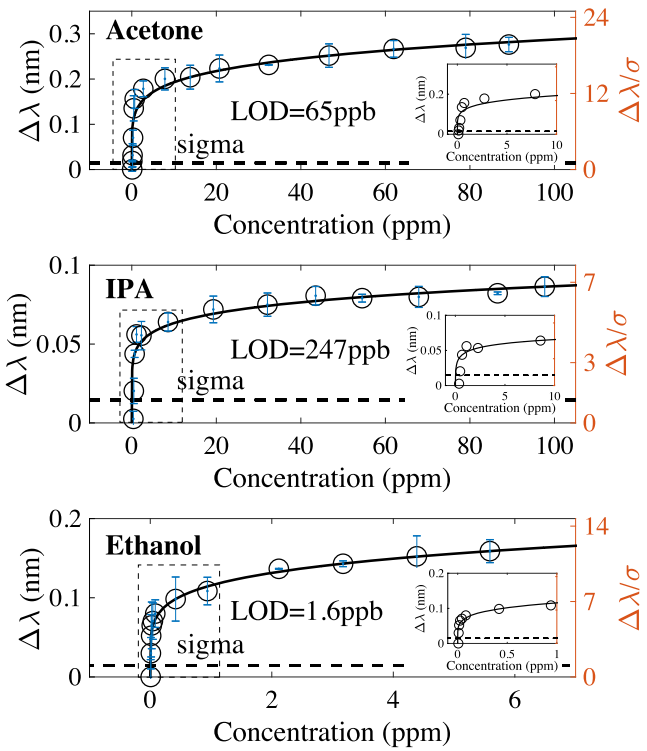

FIG. 4. Relative wavelength shift (left axis) and shift-to-noise ratio (right axis) of the MZI interference fringes as a function of gas concentrations. Data fitting was performed using the Freundlich model for multilayer mesoporous coatings. The LOD for acetone, IPA, and ethanol vapors was estimated to be 65 ppb, 247 ppb, and 1.6 ppb, respectively. Error bars come from the SD of wavelength shift values obtained upon completion of the adsorption cycle. All fits had $R^2 > 0.9$. Inset: Low-concentration plots.

of gas concentrations. This behavior can be described by the Freundlich model, which involves a multilayer adsorption with decreasing adsorption enthalpy in mesoporous silica and whose characteristic function is proportional to $c^{1/n}$, where c is the gas concentration and n is known as the Freundlich linearity index.[30] We used this model to fit the data and to derive the LOD, which we defined as the value at which the obtained fitted curves equal the measured instrumental sensitivity defined by the sigma. Following this criterion, we obtained a LOD of acetone, IPA, and ethanol to be 65 ppb, 247 ppb, and 1.6 ppb, respectively. Moreover, the associated sensitivity in the linear regime of the Freundlich model defined as $S = \sigma/\text{LOD}$ was estimated to be $S_{\text{acetone}} = 0.22$ nm/ppm, $S_{\text{IPA}} = 0.06$ nm/ppm, and $S_{\text{ethanol}} = 9.12$ nm/ppm. The difference in the measured LOD and sensitivity among the different gas analytes might be due to a number of reasons, such as the different vapor pressures and refractive index of the injected gas vapors as well as the amount of gas molecules adsorbed by the mesoporous film coating. It is of note that the high slope at low concentrations is a fundamental adsorption feature of mesoporous materials and follows the Freundlich function.

In conclusion, we demonstrated an integrated ppb-sensitive refractive index gas sensor with functionalized SiN photonic circuits. Our results show, to the best of our knowledge, the lowest reported LOD with refractive index based gas sensor devices on a silicon nitride platform. The reason for the low LOD is mainly twofold. On the one hand, the adsorption by our mesoporous silica film implies that the molecules are extracted from the gas phase and condense into the film, leading to an enrichment of the analyte. On the other hand, the long MZI sensing arm enables the light–analyte interaction length to be maximized. A low LOD is particularly useful in applications such as volatile organic compound (VOC) sensing or breath gas analysis that typically involve concentrations at a sub-100-ppb scale.[34,35] The obtained LOD may be further improved by enhancing the stability of the sensor against small mechanical drifts or thermodynamic variations so that the instrumental sensitivity would only be limited by the noise level and ultimately by the spectral resolution of the detector. To this aim, future integration of both the light source and the detector will significantly decrease the noise level, which is currently limited by a poor coupling efficiency given by the glass window of the gas cell that imposes a gap of ~2 mm from the SiN grating couplers to the input and output fibers.

In the present demonstration, the sensor stability against environmental temperature fluctuations was ensured by the controlled room temperature (22.0 °C ± 0.1 °C), the gas cell housing, the absence of heating sources (e.g., opto-electric components) as well as the low thermal coefficient of the SiN platform. At thermal equilibrium of the PIC with the surrounding environment, we expect at first approximation an estimated linear response of the demonstrated sensor in the order of ~0.005 nm/C.[36] This would impose a new spectral reference (baseline) for the sensor, yet the relative spectral response to the gas exposure would not be affected. Moreover, we envisage that the integration of one or more additional MZIs on the same chip working as references for monitoring the interferometric response to high-frequency (~0.1 Hz–1 Hz) temperature variations would ultimately remove any side effects caused by the environmental thermodynamics.[37]

Despite the unprecedented LOD in a SiN chip, our integrated MZI sensor is still limited by an intrinsically low selectivity that does not allow gathering information about the detected gas analyte. As such, further research will focus on advanced mesoporous coatings that can selectively adsorb specific gas analytes depending on their engineered porous size and functionalization. This may further enable multiplexed assays exploiting multiple MZIs on a single chip. In parallel, progress on signal enhancement on chip-scale Raman spectroscopy[38] may also provide an effective and complimentary approach for gas sensing, The maturity and flexibility of the SiN platform will allow for further electro-optic integration in the future by combining light sources and detectors on chip, paving the way to fully functionalized, compact, and portable gas sensing devices, enabling new exciting ventures for environmental safety, healthcare, and industrial processing.

The supplementary material illustrates the effect of both air flow temperature and humidity on our refractive index gas sensor.

AUTHORS' CONTRIBUTIONS

G.A. and J.G. contributed equally to the work.

The authors thank the EU pilot lines PIX4life and PIXAPP for continuous support and funding. The authors further acknowledge

© Author(s) 2020

funding from the AQUARIUS project, which has received funding from the EU Horizon 2020 Research and Innovation program under Grant Agreement No. 731465.

DATA AVAILABILITY

The data that support the findings of this study are available from the corresponding author upon reasonable request.

REFERENCES

[1] C. Di Natale, A. Macagnano, E. Martinelli, R. Paolesse, G. D'Arcangelo, C. Roscioni, A. Finazzi-Agro, and A. D'Amico, Biosens. Bioelectron. **18**, 1209 (2003).
[2] S. V. Ryabtsev, A. V. Shaposhnick, A. N. Lukin, and E. P. Domashevskaya, Sens. Actuators, B **59**, 26 (1999).
[3] C. K. Ho, M. T. Itamura, M. Kelley, and R. C. Hughes, Sandia report 28, 2001, http://citeseerx.ist.psu.edu/viewdoc/download?doi=10.1.1.499.6872&rep=rep1&type=pdf.
[4] G. Jiménez-Cadena, J. Riu, and F. X. Rius, Analyst **132**, 1083 (2007).
[5] T. Ritari, J. Tuominen, H. Ludvigsen, J. C. Petersen, T. Sørensen, T. P. Hansen, and H. R. Simonsen, Opt. Express **12**, 4080 (2004).
[6] A. Rahim, E. Ryckeboer, A. Z. Subramanian, S. Clemmen, B. Kuyken, A. Dhakal, A. Raza, A. Hermans, M. Muneeb, S. Dhoore, and R. Baets, J. Lightwave Technol. **35**, 639 (2017).
[7] A. Z. Subramanian, E. Ryckeboer, A. Dhakal, F. Peyskens, A. Malik, B. Kuyken, H. Zhao, S. Pathak, A. Ruocco, A. De Groote, and R. Baets, Photonics Res. **3**, B47 (2015).
[8] D. Martens, P. Ramirez-Priego, M. S. Murib, A. A. Elamin, A. B. González-Guerrero, M. Stehr, F. Jonas, B. Anton, N. Hlawatsch, P. Soetaert, and P. Bienstman, Anal. Methods **10**, 3066 (2018).
[9] T. Claes, J. G. Molera, K. De Vos, E. Schacht, R. Baets, and P. Bienstman, IEEE Photonics J. **1**, 197 (2009).
[10] A. Dhakal, A. Z. Subramanian, P. Wuytens, F. Peyskens, N. Le Thomas, and R. Baets, Opt. Lett. **39**, 4025 (2014).
[11] A. Raza, S. Clemmen, P. Wuytens, M. De Goede, A. S. K. Tong, N. Le Thomas, C. Liu, J. Suntivich, A. G. Skirtach, S. M. Garcia-Blanco, and R. Baets, Opt. Express **27**, 23067 (2019).
[12] H. Zhao, S. Clemmen, A. Raza, and R. Baets, Opt. Lett. **43**, 1403 (2018).
[13] E. Ryckeboer, R. Bockstaele, M. Vanslembrouck, and R. Baets, Biomed. Opt. Express **5**, 1636 (2014).
[14] D. Celo, E. Post, M. Summers, T. Smy, M. J. Brett, and J. Albert, Opt. Express **17**, 6655 (2009).
[15] N. Fabricius, G. Gauglitz, and J. Ingenhoff, Sens. Actuators, B **7**, 672 (1992).
[16] S. Ghosh and B. M. A. Rahman, J. Lightwave Technol. **35**, 3003 (2017).
[17] F. T. Dullo, S. Lindecrantz, J. Jágerská, J. H. Hansen, M. Engqvist, S. A. Solbø, and O. G. Hellesø, Opt. Express **23**, 31564 (2015).
[18] J. T. Robinson, L. Chen, and M. Lipson, Opt. Express **16**, 4296 (2008).
[19] V. Passaro, F. Dell'Olio, and F. De Leonardis, Sensors **7**, 2741 (2007).
[20] R. Orghici, P. Lützow, J. Burgmeier, J. Koch, H. Heidrich, W. Schade, N. Welschoff, and S. Waldvogel, Sensors **10**, 6788 (2010).
[21] N. A. Yebo, P. Lommens, Z. Hens, and R. Baets, Opt. Express **18**, 11859 (2010).
[22] N. A. Yebo, S. P. Sree, E. Levrau, C. Detavernier, Z. Hens, J. A. Martens, and R. Baets, Opt. Express **20**, 11855 (2012).
[23] T. H. Stievater, M. W. Pruessner, D. Park, W. S. Rabinovich, R. Andrew McGill, D. A. Kozak, R. Furstenberg, S. A. Holmstrom, and J. B. Khurgin, Opt. Lett. **39**, 969 (2014).
[24] L. Tombez, E. J. Zhang, J. S. Orcutt, S. Kamlapurkar, and W. M. J. Green, Optica **4**, 1322 (2017).
[25] S. A. Holmstrom, T. H. Stievater, D. A. Kozak, M. W. Pruessner, N. Tyndall, W. S. Rabinovich, R. Andrew McGill, and J. B. Khurgin, Optica **3**, 891 (2016).
[26] N. F. Tyndall, T. H. Stievater, D. A. Kozak, K. Koo, R. A. McGill, M. W. Pruessner, W. S. Rabinovich, and S. A. Holmstrom, Opt. Lett. **43**, 4803 (2018).
[27] See www.pix4life.eu for more information about the EU PIX4life pilot line.
[28] X. Tu, J. Song, T.-Y. Liow, M. K. Park, J. Q. Yiying, J. S. Kee, M. Yu, and G.-Q. Lo, Opt. Express **20**, 2640 (2012).
[29] D. Martens and P. Bienstman, Sci. Rep. **9**, 5767 (2019).
[30] B. Baumgartner, J. Hayden, A. Schwaighofer, and B. Lendl, ACS Appl. Nano Mater. **1**, 7083 (2018).
[31] B. Baumgartner, J. Hayden, J. Loizillon, S. Steinbacher, D. Grosso, and B. Lendl, Langmuir **35**, 11986 (2019).
[32] D. A. G. Bruggeman, Ann. Phys. **416**, 636 (1935).
[33] B. Baumgartner, J. Hayden, and B. Lendl, Sens. Actuators, B **302**, 127194 (2020).
[34] C. Jia, S. Batterman, and C. Godwin, Atmos. Environ. **42**, 2083 (2008).
[35] S. Das and M. Pal, J. Electrochem. Soc. **167**, 037562 (2020).
[36] D. Pérez, J. Fernández, R. Baños, J. D. Doménech, A. M. Sánchez, J. M. Cirera, R. Mas, J. Sánchez, S. Durán, E. Pardo *et al.*, arXiv:1604.02958 (2016).
[37] S. Dwivedi, H. D'heer, and W. Bogaerts, IEEE Photonics Technol. Lett. **25**, 2167 (2013).
[38] H. Zhao, B. Baumgartner, A. Raza, A. Skirtach, B. Lendl, and R. Baets, Opt. Lett. **45**, 447 (2020).

© Author(s) 2020